

<https://doi.org/10.1038/s42003-024-06993-x>

FUT2 promotes colorectal cancer metastasis by reprogramming fatty acid metabolism via YAP/TAZ signaling and SREBP-1



Chenfei Dong^{1,2}, Yue Zhang^{1,2}, Jiayue Zeng^{1,2}, Suli Chong^{1,2}, Yang Liu^{1,2}, Ziming Bian^{1,2}, Sairong Fan^{1,2,3} ✉ & Xiaoming Chen^{1,2} ✉

Colorectal cancer (CRC) ranks as the second most lethal cancer worldwide because of its high rate of metastasis, and approximately 20% of CRC patients have metastases at initial diagnosis. Metabolic reprogramming, a hallmark of cancer cells, has been implicated in the process of metastasis. We previously demonstrated that fucosyltransferase 2 (FUT2) promotes the malignancy of CRC cells, however, the underlying mechanisms remain unclear. Here, bioinformatic analysis revealed that FUT2 is associated with the malignant phenotype and fatty acid metabolism in CRC. FUT2 knockdown decreased glucose uptake and de novo fatty acid synthesis, which in turn inhibited the proliferation and metastasis of CRC cells. Mechanistically, FUT2 promotes YAP1 nuclear translocation and stabilizes mSREBP-1 by fucosylation, thus promoting de novo fatty acid synthesis in CRC cells. In summary, this study demonstrates that FUT2 promotes the proliferation and metastasis of CRC cells by reprogramming fatty acid metabolism via YAP/TAZ signaling and SREBP-1, indicating that FUT2 might be a potential target for developing therapeutic strategies against CRC.

Colorectal cancer (CRC) is one of the most common and second deadly cancers globally, and its incidence and mortality are increasing rapidly^{1,2}. The high mortality of CRC is due to tumor metastasis, which accounts for 90% of CRC deaths and less than 20% of the 5-year survival rates³. CRC can spread through the body and form distant metastases in the lymph nodes, lungs, liver, peritoneum and abdominal cavity⁴. Even with considerable progress in the detection and management of CRC, the survival rates for patients are still significantly low, primarily due to tumor metastasis or recurrence^{5,6}. Therefore, it is urgently necessary to clarify the underlying mechanisms of CRC metastasis and develop new therapies to improve the outcomes of CRC patients. Metabolic reprogramming is commonly observed in cancers, and recognized as a hallmark of cancer⁷. Among these dysregulated metabolic pathway, abnormal lipid metabolism plays a major role in tumorigenesis and metastasis⁸. Lipid metabolic reprogramming provides cancer cells with components for the synthesis of cellular membranes, generation of energy, and signal transduction^{9,10}. Research has showed that dysregulated lipid metabolism plays a vital role in facilitating

CRC invasion and metastasis^{11,12}. However, the mechanisms underlying the reprogramming of lipid metabolism in CRC remain poorly understood.

Glycosylation, a ubiquitous and essential post-translational modification, plays crucial roles in cell growth, cell adhesion, immune tolerance, and metabolic reprogramming etc^{13,14}. Accumulating evidences show that aberrant glycosylation, a common feature of cancer cells, plays important roles in metabolic reprogramming in cancer^{15,16}. Researchers have shown that fucosyltransferases are abnormally regulated in CRC and linked to multiple aspects of cancer pathology¹⁷. Our prior research revealed that fucosyltransferase 2 (FUT2), which is responsible for the addition of fucose to the α -1, 2 linkage at glycan termini, was upregulated in CRC, and promoted the progression of CRC¹⁸. However, the role of FUT2 in CRC metastasis is unclear.

The Hippo signaling pathway, an evolutionarily conserved pathway, regulates multiple biological processes and plays an important role in the tumorigenesis and metastasis of cancer, including metabolic reprogramming¹⁹. As a key regulator of the Hippo pathway, YAP is

¹Key Laboratory of Laboratory Medicine, Ministry of Education, School of Laboratory Medicine and Life Sciences, Wenzhou Medical University, Wenzhou, China.

²Institute of Glycobiological Engineering, School of Laboratory Medicine and Life Sciences, Wenzhou Medical University, Wenzhou, China. ³Wenzhou Key Laboratory of Cancer Pathogenesis and Translation, School of Laboratory Medicine and Life Sciences, Wenzhou Medical University, Wenzhou, China.

✉ e-mail: fansairong@wmu.edu.cn; xmc@wmu.edu.cn

predominantly regulated by phosphorylation²⁰. When Hippo signaling is activated, YAP is inactivated by phosphorylation and constrained in the cytoplasm. In contrast, when Hippo is inactive, YAP is activated by dephosphorylation and shuttled into the nucleus²¹. Recently, studies have indicated that YAP plays important role in metabolic regulation, such as lipogenesis, fatty acid degradation, glycolysis and glutamate decomposition, and has received increasing attention of the metabolism reprogramming in cancer cells²². The effect of YAP nuclear-cytoplasmic transport can be regulated by phosphorylation, methylation, ubiquitination, and glycosylation. The OGT-mediated glycosylation of YAP induces YAP dephosphorylation and activation to promote tumor growth and metastasis²³. The polypeptide N-acetylgalactosaminyltransferase 12 (GALNT12) promotes YAP1 nuclear translocation, which activates key downstream genes, therefore promoting fibrosarcoma growth²⁴.

In this study, we confirmed that upregulated FUT2 was associated with lipid metabolism in CRC. FUT2 promoted the transcription of glucose transporter type 1 (GLUT1) and fatty acid synthases through YAP/TAZ signaling, through which YAP1 was dephosphorylated and activated by fucosylation in CRC cells. Additionally, the fucosylation of mSREBP-1 by FUT2 enhances its stability, further promoting de novo fatty acid synthesis, thereby promoting CRC metastasis. This study provides new insight into the mechanism of lipid metabolism in CRC and potential targets for future therapies.

Results

FUT2 is upregulated in CRC and correlated with clinical outcomes

We previously reported that FUT2 is upregulated in clinical CRC tissue, compared with matched normal tissues from the same patients¹⁸. Here, the data from The Cancer Genome Atlas (TCGA) and Genote-Tissue Expression (GTEx) databases revealed that FUT2 gene expression is elevated in CRC tumors compared with normal colorectal tissues (Fig. 1A). Immunohistochemistry results from the Human Protein atlas (HPA) database also revealed that FUT2 was significantly elevated in CRC tissues compared with normal tissues (Fig. 1B). Additionally, receiver operating characteristic (ROC) curve analysis revealed that FUT2 had an area under the curve (AUC) value of 0.78 (sensitivity 98%, specificity 55%) (Fig. 1C), indicating that FUT2 could aid in the diagnosis of CRC. On the basis of the expression levels of FUT2, the correlation between FUT2 and CRC clinical parameters was investigated via the chi-square test. The results revealed that the expression of FUT2 was associated with race, M stage, N stage, and pathologic stage (Supplementary Table 1). The stromal and ESTIMATE scores were higher in the high-FUT2 expression group than in the low-FUT2 expression group, while no notable variance was observed in the immune scores (Fig. 1D). To further investigate the role of FUT2 in the tumor microenvironment, we analyzed the single-cell RNA (scRNA) sequence dataset GSE146771 from the Tumor Immune Single-cell Hub (TISCH) database. TSNE plots displayed thirteen distinct cell clusters (Fig. 1E), in which FUT2 was predominantly localized in malignant tumor cells (Fig. 1F, G). Notably, elevated fatty acid metabolism was also detected in malignant tumor cells (Fig. 1H). Expanding our investigation to TCGA-CRC patients, we found that the lipid metabolism pathway significantly impacts CRC prognosis in high-risk patients (Supplementary Fig. 1A–D). Furthermore, gene set enrichment analysis (GSEA) demonstrated that FUT2 was positively correlated with fatty acid metabolism in CRC patients ($P = 0.00052$, NES = 1.78) (Fig. 1I). These findings suggest that FUT2 is associated with fatty acid metabolism in CRC.

FUT2 enhances fatty acid synthesis in CRC cells

To investigate the biological role of FUT2 in lipid metastasis in CRC cells, specific shRNAs targeting FUT2 were introduced into SW480 and DLD-1 cells to silence FUT2 expression in CRC cells, and the effects were assessed by Western blot. Compared with that in NC cells, the expression of FUT2 in sh-FUT2 cells was significantly lower (Fig. 2A). To ensure that the fucosylation was catalyzed by FUT2, not FUT1, which also catalyze the addition

of alpha 1, 2-linked fucose to glycans, the expression of FUT1 was investigated. As shown in Fig. 2B, the expression of FUT1 was not affected by FUT2 knockdown. FUT2 knockdown significantly decreased the intracellular levels of triglyceride (TG), total cholesterol (T-CHO) and free fatty acid (FFA) in SW480 and DLD-1 cells (Fig. 2C). The lipid content, as detected by the fluorescent lipophilic stain Nile Red, revealed that FUT2 knockdown significantly reduced the neutral lipids in SW480 and DLD-1 cells (Fig. 2D). Additionally, FUT2 knockdown markedly reduced the levels of TG and T-CHO in subcutaneous tumor models (Fig. 2E). To investigate whether the FUT2 induced increase in lipid accumulation was due to its regulation of the de novo fatty acid synthesis pathway, the key enzymes involved in de novo fatty acid synthesis were examined. As shown in Fig. 2F, knockdown of FUT2 significantly decreased the expression of acetyl-CoA carboxylase α (ACC 1), ATP citrate lyase (ACLY), carnitine palmitoyltransferase 1A (CPT1A), and fatty acid synthetase (FASN), whereas the levels of adipose triglyceride lipase (ATGL) were markedly increased in both SW480 and DLD-1 cells. These results indicate that FUT2 enhances de novo fatty acid synthesis in CRC cells.

FUT2 promotes CRC cell growth and metastasis by enhancing fatty acid synthesis

The reprogramming of fatty acid metabolism can accelerate the development and progression of CRC²⁵. To further explore whether FUT2-mediated fatty acid synthesis promotes CRC cell growth and metastasis, palmitic acid, the most common long-chain fatty acid, was used. The results showed that palmitic acid treatment markedly promoted cell proliferation and colony formation, which were significantly attenuated by FUT2 knockdown (Fig. 3A, B). As shown in Fig. 3C, FUT2 knockdown markedly suppressed palmitic acid-induced migration and invasion of CRC. Overexpression of FUT2 significantly increased the migration and invasion of CRC cells (Fig. 3D and Supplementary Fig. 2). Meanwhile, treated with orlistat, a fatty acid synthase inhibitor, the migration and invasion of CRC cells were significantly reduced with or without FUT2 overexpression. These results suggest that FUT2 promotes CRC cell growth and metastasis by enhancing fatty acid synthesis.

Elevated levels of membrane lipid rafts, which affect signaling and protein localization at the cell membrane, in turn affect the dynamics of the cytoskeleton, which plays a crucial role in tumor progression, including migration, invasion, and colonization at new sites^{26,27}. Phalloidin staining revealed that FUT2 knockdown significantly reduced cytoskeleton formation (Fig. 3E), and FUT2 overexpression increased cytoskeleton formation (Fig. 3F). The FUT2-mediated increase in cytoskeleton formation was significantly reduced by orlistat treatment (Fig. 3F). The results showed that blocking fatty acid synthesis significantly inhibited cytoskeleton formation, confirming the role of FUT2 in the regulation of lipid metabolism in CRC cells.

Dysregulated fatty acid metabolism can cause cellular stress, such as oxidative stress, which in turn affects cytoskeletal stability and cell viability²⁸. The results revealed that FUT2 knockdown significantly increased the levels of ROS and MDA (Fig. 4A, B). Moreover, FUT2 knockdown markedly decreased the level of cellular glutathione (GSH), an essential antioxidant that protects cells against various forms of prooxidants and free radicals (Fig. 4C). Increased lipid peroxidation is lethal to cells, whereas ferroptosis, a form of non-apoptotic cell death, is triggered by excessive lipid peroxidation-induced damage and iron accumulation²⁹. To further investigate the role of FUT2 in CRC, the effect of FUT2 on ferroptosis was detected. FUT2 knockdown significantly decreased the expression of FTH and GPX4 and increased the expression of TFR1 (Fig. 4D). We further evaluated the role of FUT2 in ferroptosis by assessing RSL3-induced ferroptosis with or without ferrostatin-1 (Fer-1), an inhibitor of ferroptosis. FUT2 knockdown significantly increased the MDA production of RSL-3 treated SW480 cells (Fig. 4E), whereas FUT2 overexpression markedly decreased the MDA production of RSL-3 treated SW480 cells (Fig. 4F). Moreover, after Fer-1 treated, the MDA production of SW480 cells was not affected by FUT2 knockdown or overexpression. Induction of cellular

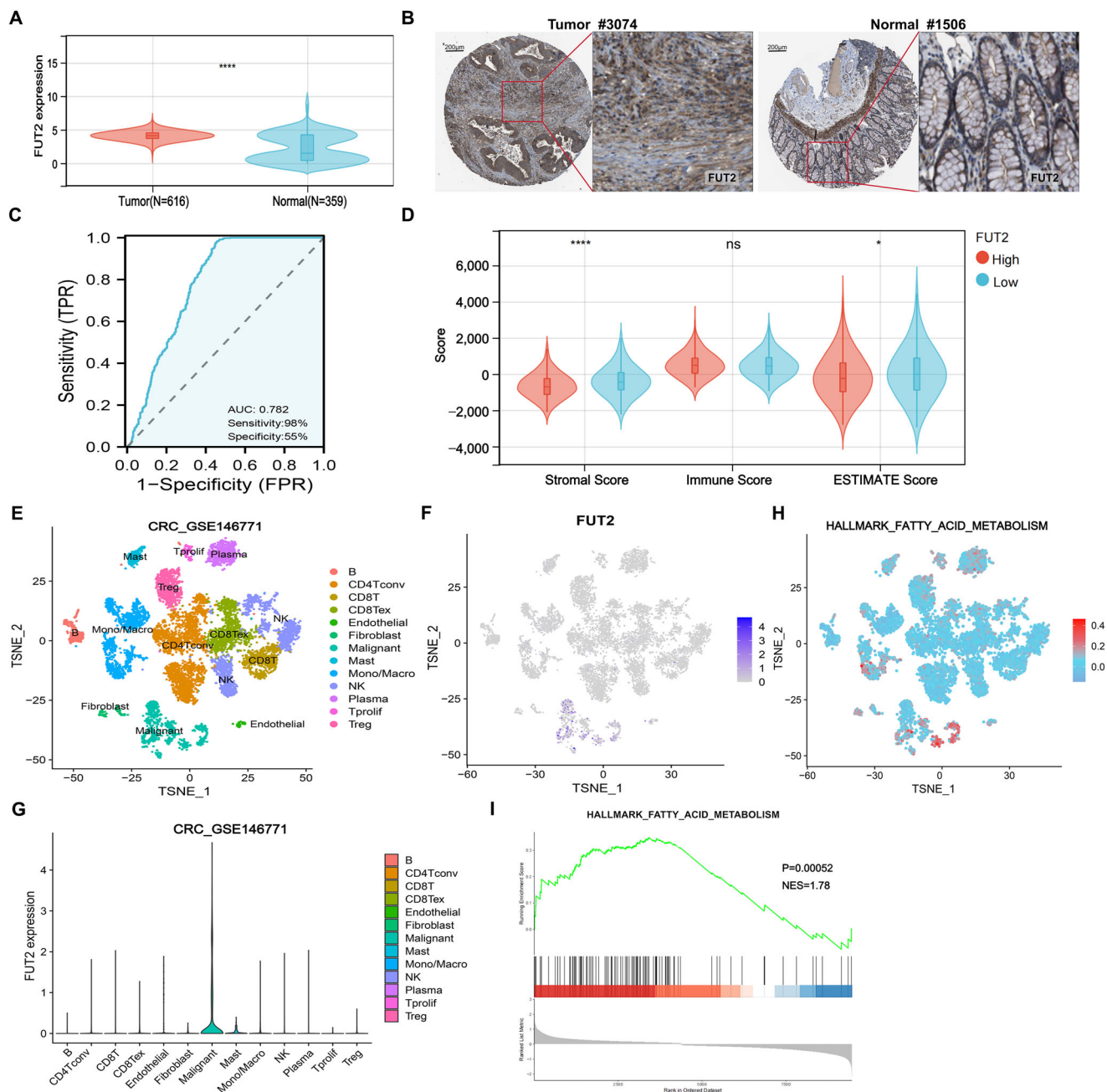


Fig. 1 | Bioinformatic analysis of the expression of FUT2 and fatty acid metabolism in CRC. **A** The mRNA levels of FUT2 in normal ($n = 359$) and CRC ($n = 616$) specimens were quantified. Relevant data processing details of the specimens were provided in the methods section. **B** Representative immunohistochemistry (IHC) images from the Human Protein Atlas (HPA) illustrating the expression of FUT2 in CRC and normal tissues. Scale bar represents 200 μm . **C** Receiver operating characteristic (ROC) curve analysis of *FUT2* mRNA expression in CRC ($n = 975$), showing an AUC of 0.782, with a sensitivity of 98% and specificity of 55%. Relevant data processing details were provided in the methods section. **D** Tumor microenvironment (TME) score categorized by the expression levels of FUT2 in the TCGA-CRC dataset, indicating its correlation with the stromal score. Relevant data processing details were provided in the methods section. **E** TSNE plot illustrating cell type clustering in the GSE146771 dataset, highlighting the distribution of various cell populations. Relevant data processing details were provided in the methods section.

F TSNE plot depicting the distribution of FUT2 expression across different cell subsets within the GSE146771 dataset, indicating its correlation with malignancy. Relevant data processing details were provided in the methods section. **G** Violin plot representing *FUT2* expression at the single-cell level within the GSE146771 dataset, showing variability among different cell types. Relevant data processing details were provided in the methods section. **H** TSNE plot of the gene set associated with fatty acid metabolism across cell subsets within the GSE146771 dataset, providing insights into metabolic reprogramming. Relevant data processing details were provided in the methods section. **I** GSEA comparing high and low *FUT2* expression groups in the TCGA-CRC dataset, revealing a significant enrichment of fatty acid metabolism pathways ($P = 0.00052$, $\text{NES} = 1.78$). Relevant data processing details were provided in the methods section. Statistical significance was determined using Wilcoxon rank test, with $*p < 0.05$, $****p < 0.0001$, ns: not significant.

ferroptosis has already been shown to overcome cancer resistance to cisplatin³⁰. We further investigated the impact of *FUT2* on CRC cells following treatment with cisplatin by viability assays. Notably, *FUT2* knock-down enhanced the sensitivity of CRC cells to cisplatin (Fig. 4G).

FUT2 promotes the migration and invasion of CRC cells via YAP/TAZ signaling
To investigate the underlying mechanism of *FUT2* in CRC, GO and KEGG enrichment analyses were conducted on genes differentially expressed in

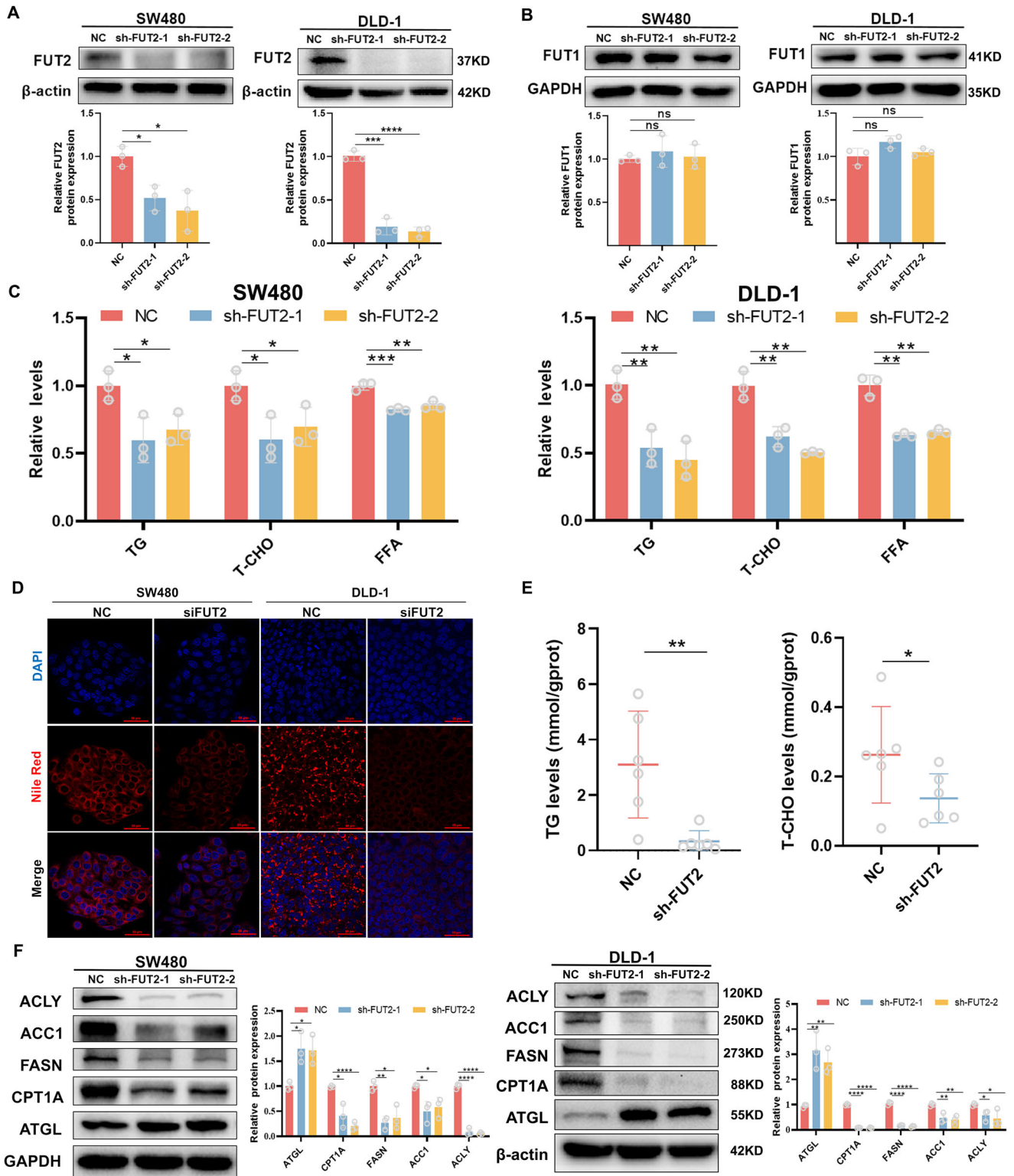
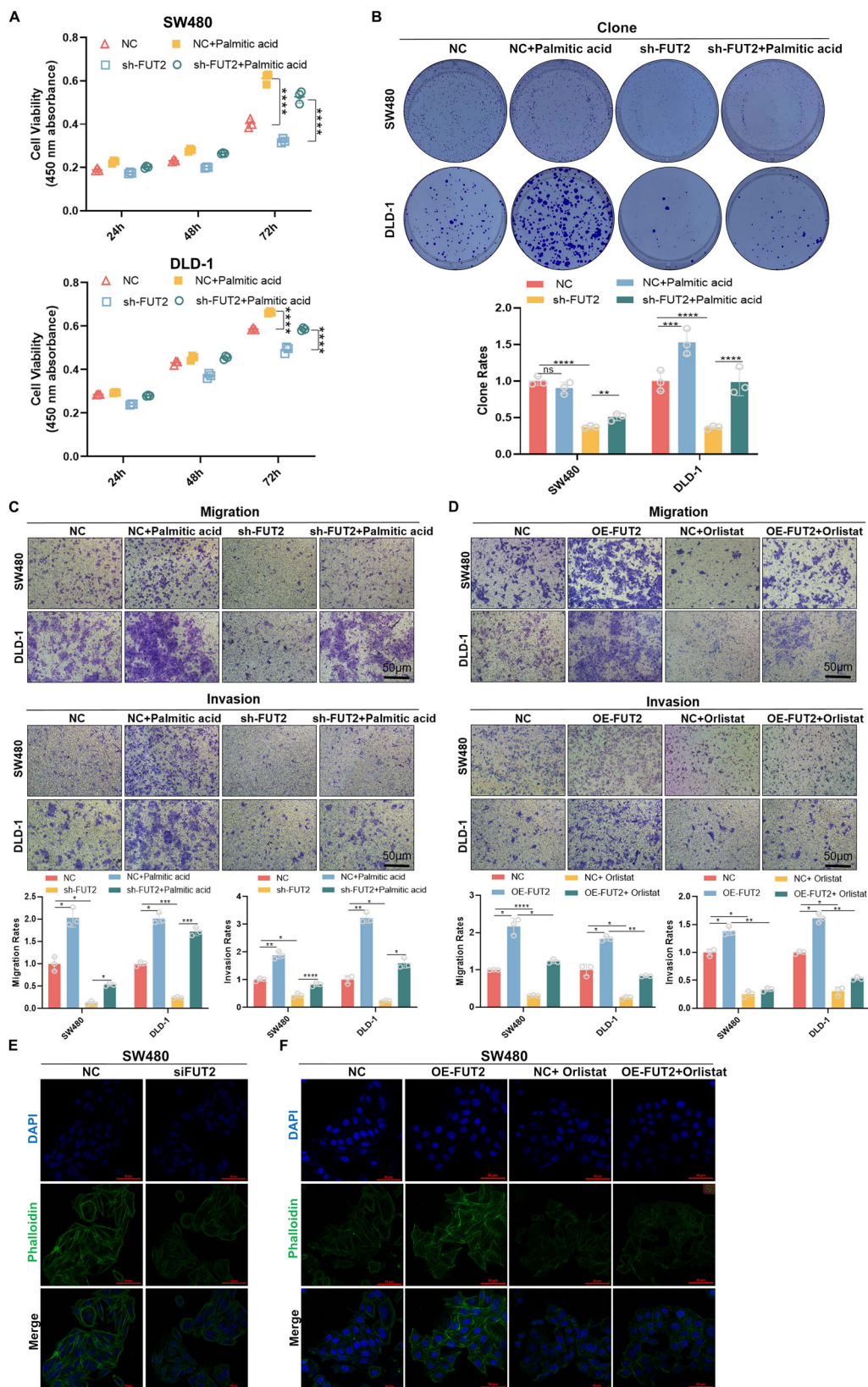


Fig. 2 | FUT2 knockdown inhibits lipid synthesis in CRC cells. **A** SW480 and DLD-1 cells were stably transfected with FUT2-shRNA, and then western blot analysis of FUT2 (**A**)/FUT1 (**B**) expression was determined. The relative density of protein bands was quantified, normalized to β -actin/GAPDH, and fold changes were shown in histograms from three independent experiments. **C** SW480 and DLD-1 cells were transfected with FUT2-siRNA, and the levels of TG, T-CHO, and FFA were detected. Data shown are mean \pm SD; $n = 3$ samples. **D** SW480 and DLD-1 cells were transfected with FUT2-siRNA, and then stained with Nile red to evaluate intracellular neutral lipid accumulation. Red fluorescence signals were captured and visualized through a fluorescent microscope using constant fluorescence parameters explained in the methods section: scale bar, 50 μ m. **E** BALB/c nude mice were

subcutaneously implanted with the FUT2-knockdown (sh-FUT2) or control (NC) SW480 cells. After 30 days of transplantation, the levels of TG and T-CHO in tumor specimens ($n = 6$ mice/group) were detected. **F** SW480 and DLD-1 cells were transfected with FUT2-shRNA, and then western blot analysis of key lipid metabolism enzymes, including ACLY, ACC1, FASN, CPT1A, and ATGL expressions were determined. The relative density of protein bands was quantified, normalized to β -actin or GAPDH, and fold changes were shown in histograms from three independent experiments. Statistical significance was determined using one-way ANOVA using the Bonferroni post-hoc test, with * $p < 0.05$, ** $p < 0.01$, *** $p < 0.001$, **** $p < 0.0001$, ns: not significant.



relation to FUT2 in the TCGA-CRC dataset. GO analysis revealed that FUT2 was associated with cell adhesion, regulation of the actin cytoskeleton, and fatty acid synthesis (Fig. 5A), and KEGG analysis revealed that FUT2 was significantly linked to the Hippo pathway (Fig. 5B). To confirm this, key factors of the Hippo pathway, including CTGF and CYR61, which are

critical in the metastatic process of tumor cells, were tested. FUT2 knock-down had no effect on the expression of YAP1 or LATS1 in SW480 cells, whereas the expression of TAZ, CTGF and CYR61 was significantly reduced, and the phosphorylation of YAP1 (Ser127) was significantly increased (Fig. 5C). Additionally, the effects of FUT2 on YAP1 distribution

Fig. 3 | FUT2-mediated fatty acid synthesis promotes CRC cell proliferation and metastasis. SW480 and DLD-1 cells were transfected with FUT2-shRNA, and then CCK8 assay (A) and colony formation assay (B) were performed to assess the proliferative capacity of cells with or without 50 μ M palmitic acid. Data shown are mean \pm SD; $n = 3$ samples. SW480 and DLD-1 cells transfected with FUT2-shRNA or FUT2/Lv105. After transfection, cells were treated with 50 μ M palmitic acid (C) or 50 μ M orlistat (D) for 24 h and then transwell assay was performed. The number of migrating/invading cells was quantified using Image J software. Scale bar represents 50 μ m. Data shown are mean \pm SD; $n = 3$ samples. E SW480 cells were transiently transfected with FUT2-siRNA, and then stained with phalloidin to evaluate

intracellular cytoskeleton organization. Green fluorescence signals were captured and visualized through a fluorescent microscope using constant fluorescence parameters explained in the methods section: scale bar, 50 μ m. F SW480 cells were transiently transfected with FUT2/Lv105. After transfection, the cells were treated with orlistat (50 μ M) for 24 h, and then stained with phalloidin to evaluate intracellular cytoskeleton organization. Green fluorescence signals were captured and visualized through a fluorescent microscope using constant fluorescence parameters explained in the methods section: scale bar, 50 μ m. Statistical significance was determined using one-way ANOVA using the Bonferroni post-hoc test, with * $p < 0.05$, ** $p < 0.01$, *** $p < 0.001$, **** $p < 0.0001$, ns: not significant.

were analyzed via a cell fractionation assay. Compared with NC, FUT2 knockdown significantly decreased the nuclear fraction of YAP1 and increased the cytoplasmic fraction of YAP1 in SW480 cells (Fig. 5D), indicating that FUT2 promotes YAP1 translocation into the nucleus. The level of TAZ in the nucleus was significantly decreased in FUT2 knockdown SW480 cells, compared with that in NC cells (Fig. 5D). The expression of CTGF, a downstream factor of the YAP/TAZ signaling, was significantly reduced by FUT2 knockdown or YAP1/TAZ knockdown (Fig. 5E, F). Verteporfin, an inhibitor of YAP1, was used to investigate whether FUT2 promotes CRC cell metastasis through YAP/TAZ signaling. As shown in Fig. 5G, the migration and invasion of CRC cells were significantly reduced in simultaneously knockdown of FUT2 and verteporfin treatment CRC cells, compared with that in knockdown FUT2 or verteporfin treatment CRC cells. Overexpression of FUT2 increased the migration and invasion of CRC cells, which was significantly suppressed by verteporfin treatment (Fig. 5H). These findings suggest that FUT2 promotes the migration and invasion of CRC cells through the YAP/TAZ signaling, at least partially.

YAP1 nuclear transport is regulated by fucosylation

To investigate whether YAP1 was fucosylated by FUT2, co-immunoprecipitation and lectin blotting analysis were performed. Co-immunoprecipitation experiment showed that FUT2 was interacts directly with YAP1, but not with TAZ (Fig. 6A). The UEA-1 pull-down assays showed that the fucosylation of YAP1 was markedly reduced by FUT2 knockdown (Fig. 6B), and the glycosylation sites on YAP1 was predicted via the NetNGlyc1.0 online tool (Fig. 6C). To further validate the role of fucosylation in YAP1, cells were treated with 2F-Peracetyl-Fucose (2F-PAF), a specific inhibitor of fucosylation. Results showed that fucosylation of YAP1 was significantly decreased by 2F-PAF treatment (Fig. 6B). Meanwhile, the phosphorylation of YAP1 was increased and the expression of CTGF was decreased by 2F-PAF treatment (Fig. 6D). These results suggest that the effect of YAP1 was regulated by FUT2-mediated fucosylation.

FUT2 promotes fatty acid synthesis via YAP/TAZ signaling

To investigate whether FUT2 regulates lipid metabolism via YAP/TAZ signaling, we assessed the expression of key enzymes involved in lipid metabolism. Western blot analysis revealed that YAP1 knockdown led to a decrease in the expression of FASN and CPT1A, whereas ATGL expression remained unaffected (Fig. 6E). Quantitative real-time PCR (qRT-PCR) results showed that the mRNA expression of FASN and CPT1A was significantly decreased by YAP1 knockdown (Fig. 6F). Furthermore, the functional impact of YAP/TAZ signaling on lipid synthesis and cytoskeleton formation was investigated. Treated with verteporfin, the lipid synthesis and cytoskeleton formation of CRC cells were significantly impaired (Fig. 6G, H). Overexpression of FUT2 promoted both lipid synthesis and cytoskeleton formation in SW480 cells, and these effects were suppressed by verteporfin treatment. Furthermore, the results showed that the expression of FASN, ACC1, and TAZ was decreased, and the p-YAP1 was increased in knockdown FUT2 nude mice xenografts models (Fig. 6I, J). These results suggest that FUT2 regulates fatty acid synthesis via YAP/TAZ signaling.

FUT2 promotes fatty acid synthesis by increasing glucose uptake in CRC cells

The main raw material for lipid synthesis is derived from the products of cellular glucose metabolism¹¹. Research has shown that the expression of GLUT1, a major glucose transporter, is regulated by the Hippo pathway³¹. Here, we found that YAP1 (or FUT2) knockdown significantly decreased the mRNA expression of GLUT1 in SW480 cells (Fig. 7A, B). The western blot results revealed that FUT2 knockdown significantly decreased GLUT1 expression in CRC cells (Fig. 7C). To further verify the regulatory effect of FUT2 on GLUT1, the total cellular levels of glucose (Glu) were examined. The results revealed that the level of glucose was markedly decreased by FUT2 knockdown in CRC cells (Fig. 7D). We therefore hypothesized that FUT2 affects glucose uptake capacity, which in turn affects lipid synthesis. To determine whether glucose restriction affects fatty acid synthesis, we treated SW480 cells with medium containing either 25 mM or 5 mM glucose. The results revealed that the levels of TG and glucose were markedly lower in FUT2-knockdown cells treated with 25 mM or 5 mM glucose than in the corresponding control cells. High glucose treatment significantly increased the level of TG; however, there was no significant difference in the level of TG between 25 mM and 5 mM glucose treated in FUT2 knockdown SW480 cells (Fig. 7E). Interestingly, compared with the corresponding controls, FUT2 knockdown markedly reduced the intracellular levels of ATP under both 25 mM and 5 mM glucose conditions, whereas compared with FUT2 knockdown, the level of ATP was no significant different under different concentrations of glucose (Fig. 7E). Moreover, FASN expression was significantly decreased with FUT2 knockdown under glucose limitation (Fig. 7F). The results indicated that the conversion of glucose to TG was inhibited by FUT2 knockdown in SW480 cells.

Changes in gene expression are coordinately regulated at the level of the transcriptional pathway by transcription factors, where the transcription factors carbohydrate response element-binding protein (ChREBP) and max-like protein X (MLX) bind and activate triglyceride synthesis genes in a glucose-dependent manner^{32,33}, among which, SREBP-1 (sterol regulatory element binding protein 1) predominantly regulates fatty acid de novo synthesis genes³⁴. By further examining the mRNA levels of the above transcription factors and fatty acid synthesis genes in cells under high glucose conditions, we found that FUT2 knockdown mainly passively affected the expression of SREBP-1 under glucose limitation (Fig. 7G). Taken together, these results indicate that FUT2 enhances the transcription of GLUT1 via YAP/TAZ signaling and thereby enhances the glucose uptake capacity of CRC cells, which in turn promotes fatty acid synthesis.

Fucosylation of mSREBP-1 regulated by FUT2 enhances mSREBP-1 stability

The SREBP-1 precursor (pSREBP-1) located in the endoplasmic reticulum is activated to enter the Golgi apparatus for shear processing to form mature SREBP-1 (mSREBP-1), which is translocated to the nucleus and promotes the transcription of genes involved in de novo lipogenesis by binding to specific sterol regulatory elements (SREs)³⁵. As shown in Fig. 8A, FUT2 knockdown did not affect the expression of pSREBP-1, whereas the level of mSREBP-1 was markedly decreased by FUT2 knockdown in SW480 cells. The mRNA levels of SREBP-1 downstream factors, including ACC1, FASN, SCD,

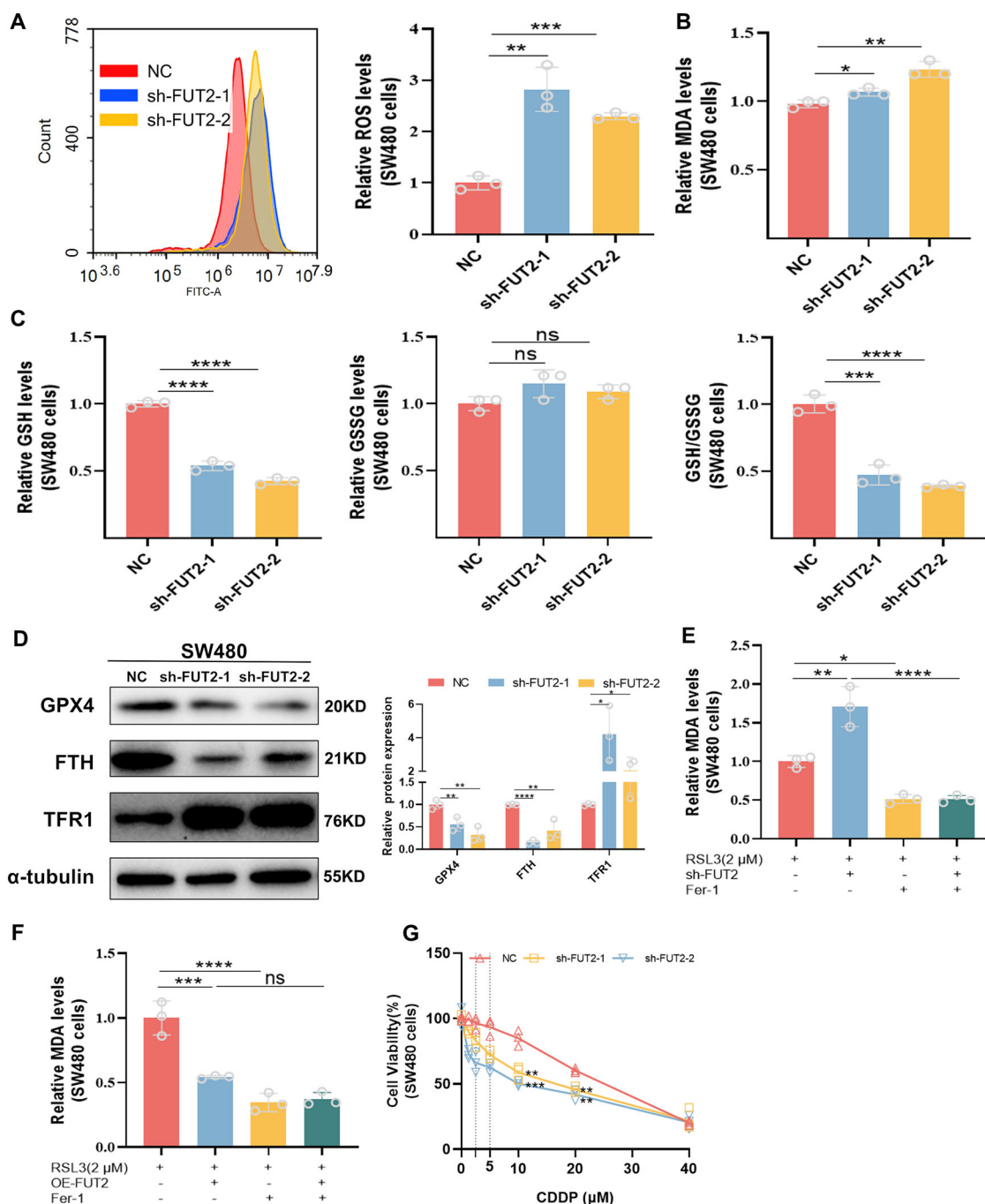
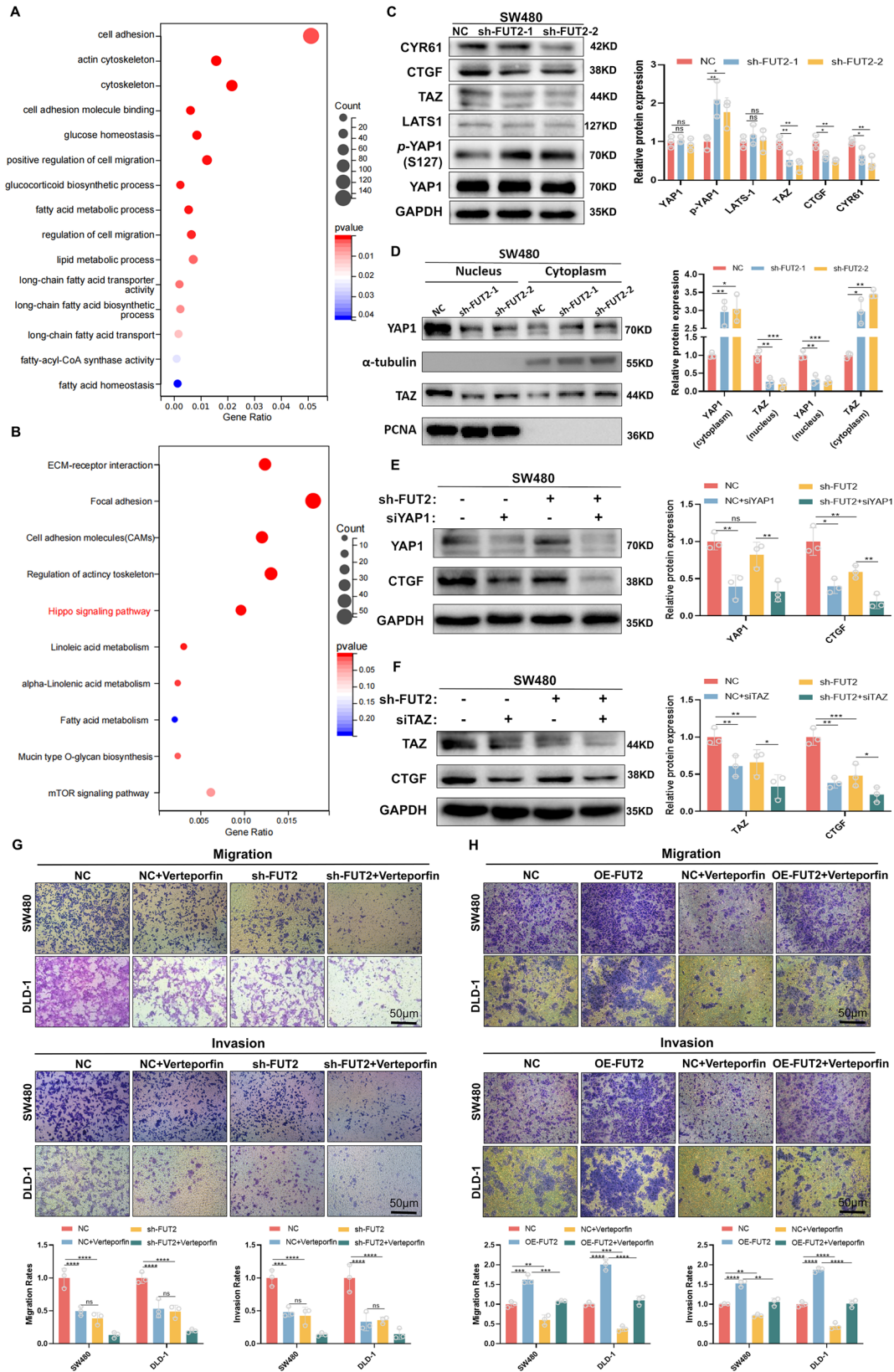


Fig. 4 | FUT2 suppresses the ferroptosis of CRC cells. A SW480 and DLD-1 cells were transfected with FUT2-shRNA, and then the ROS level was assessed by flow cytometry. The bar graph showing ROS level was expressed as a percentage of the control. Data shown are mean ± SD; *n* = 3 samples. B, C SW480 cells were transfected with FUT2-shRNA, and then the levels of MDA, GSH and glutathione disulfide (GSSG) levels were assessed. Data shown are mean ± SD; *n* = 3 samples. D SW480 cells were transfected with FUT2-shRNA, and then western blot analysis of key ferroptosis markers, including GPX4, FTH, and TFR1 expressions were determined. The relative density of protein bands was quantified, normalized to α-tubulin, and fold changes were shown in histograms from three independent

experiments. SW480 cells were transiently transfected with FUT2-shRNA (E) or FUT2/Lv105 (F). After transfection, the cells pre-treated with RSL3 (2 μM) were treated with ferrostatin (Fer-1) (1 μM) for 24 h, and then the level of MDA was determined. Data shown are mean ± SD; *n* = 3 samples. G Cell viability assay in SW480 cells treated with indicated concentrations of cisplatin for 24 h, showing that FUT2 expression modulates cisplatin sensitivity. Data shown are mean ± SD; *n* = 3 samples. Statistical significance was determined using one-way ANOVA using the Bonferroni post-hoc test, with **p* < 0.05, ***p* < 0.01, ****p* < 0.001, *****p* < 0.0001, ns: not significant.

HMGCR, *HMGCS*, and *INSIG1* were markedly decreased by FUT2 knockdown (Fig. 8B). Co-immunoprecipitation results showed that there is an interaction between FUT2 and mSREBP-1 (Fig. 8C). Lectin UEA-1 assays revealed that both FUT2 knockdown or fucosylation inhibitor treatment significantly reduced the fucosylation of

mSREBP-1 (Fig. 8D), and NetNGlyc1.0 online predicted the presence of glycosylation sites of SREBP-1 (Fig. 6C). To further determine how FUT2 stabilizes the mSREBP-1 protein, the protein synthesis inhibitor cycloheximide (CHX) and the proteasome inhibitor MG-132 were used to test the degradation pathway of mSREBP-1. The results



revealed that the mSREBP-1 content was markedly decreased by FUT2 knockdown with CHX treatment (Fig. 8E). MG132 treatment can prevent the degradation of mSREBP-1 by FUT2 knockdown (Fig. 8F), indicating that FUT2 stabilizes mSREBP-1 by protecting it from proteasome degradation.

Furthermore, JASPER analysis revealed that TEADs and SREBP-1 have close binding sites in the *FASN* promoter region (Fig. 8G). Co-IP experiments revealed an interaction between YAP1 and mSREBP-1 (Fig. 8H). These results suggest that the interaction of YAP1 and SREBP-1 can promote the transcription of *FASN*.

Fig. 5 | FUT2 promotes CRC cell migration and invasion via YAP/TAZ signaling pathway. A total of 2910 genes regulated by FUT2 were generated from the TCGA-CRC dataset, and then GO (A) and KEGG (B) pathway enrichment analyses of 2910 genes were performed. Relevant data processing details are provided in the Methods section. C SW480 cells were transfected with FUT2-shRNA, and then western blot analysis of CYR61, CTGF, TAZ, LATS1, p-YAP1, and YAP1 expressions were determined. The relative density of protein bands was quantified, normalized to GAPDH, and fold changes were shown in histograms from three independent experiments. D SW480 cells were transfected with FUT2-shRNA, and then western blot analysis of the intracellular distribution of YAP1 and TAZ expressions were determined. The relative density of protein bands was quantified, normalized to α -tubulin or PCNA, and fold changes were shown in histograms from three

independent experiments. SW480 cells were transfected with FUT2-shRNA, YAP1-siRNA (E) or TAZ-siRNA (F), and then western blot analysis of CTGF expressions were determined. The relative density of protein bands was quantified, normalized to GAPDH, and fold changes were shown in histograms from three independent experiments. SW480 and DLD-1 cells were transfected with FUT2-shRNA (G) or FUT2/Lv105 (H). After transfection, the cells were treated with Verteporfin (500 nM) for 24 h, and then transwell assay was performed. The number of migrating/invading cells was quantified via Image J software. Scale bar represents 50 μ m. Data shown are mean \pm SD; $n = 3$ samples. Scale bar represents 50 μ m. Statistical significance was determined using one-way ANOVA using the Bonferroni post-hoc test, with * $p < 0.05$, ** $p < 0.01$, *** $p < 0.001$, **** $p < 0.0001$, ns: not significant.

Prognostic value of *FUT2*, *FASN*, *SREBP-1* and *YAP1* in CRC

Owing to the diversity in clinical presentation and individual differences in disease progression in colorectal cancer, accurate prognostic prediction for CRC patients is crucial for clinical management. Precise prognostic assessment not only aids in formulating personalized treatment, but also optimizes resource allocation, enhances treatment efficacy, and improves the quality of patients' life. By identifying key genes and signaling pathways associated with disease progression and prognosis, and integrating the expression information of multiple biomarkers, a more accurate prognostic model can be constructed. When individual genes such as *YAP1* and *SREBP-1* were evaluated as prognostic markers for CRC patients, no significant difference in overall survival (OS) was observed between the high- and low-expression groups (Supplementary Fig. 3A–D). However, by combining *YAP1*, *SREBP-1*, *FUT2*, and *FASN* into a prognostic model via LSASSO regression, distinct risk categories were established. The OS of patients in the high-risk group was significantly shorter than that of patients in the low-risk group (Fig. 8I). The model demonstrated prognostic accuracy, with concordance indices of 0.57, 0.57, and 0.71 for predicting OS at 1, 3, and 5 years, respectively (Fig. 8J). These results provide a potential model for CRC prognostic diagnosis and offer a valuable reference for further development and application of molecular biomarkers in assessing CRC prognosis.

Discussion

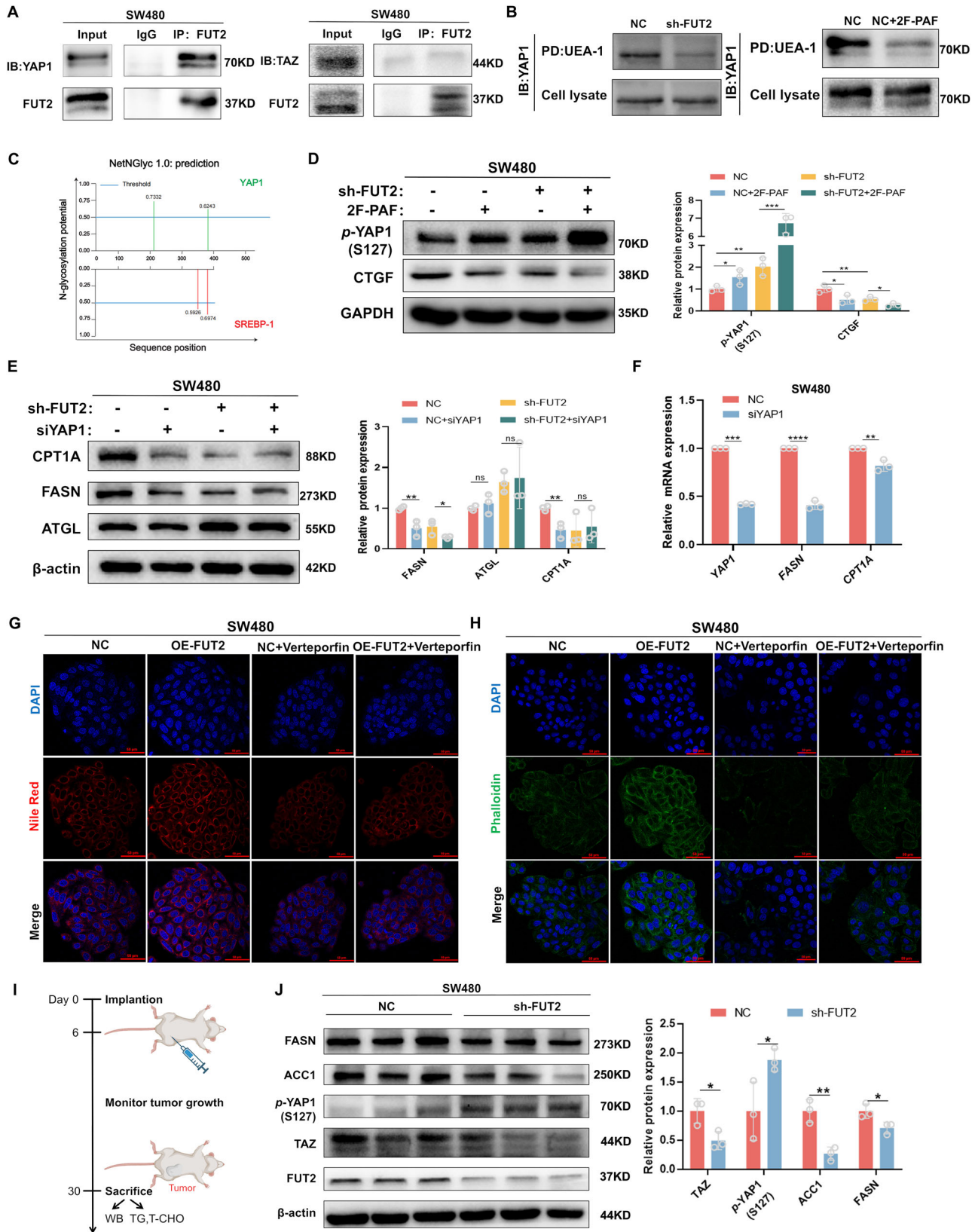
CRC is highly lethal due to distant metastases; 20% of CRC patients present with distant metastases at initial diagnosis and more than 30% of patients eventually develop metastases, with a 5-year survival rate of less than 20%³⁶. Glycosylation has emerged as an important regulator in the process of metastasis³⁷. Accordingly, the dysregulation of glycosyltransferases has been extensively studied in CRC, and altered gene expression of glycosyltransferases, as well as mutations, has been described for CRC tumor tissues and cell lines³⁸. Our previous study revealed that *FUT2* was upregulated in CRC and acted as an oncogene in the progression of CRC, and knockdown of *FUT2* markedly suppressed cell proliferation, colony formation, migration and invasion¹⁸. Surprisingly, it was reported that *FUT2* inhibited cell proliferation, invasion and tumor metastasis of CRC³⁹. Here, we found that high expression of *FUT2* in CRC can significantly distinguish between cancerous and non-cancerous tissues, and is linked to increased stromal and ESTIMATE scores, indicating that *FUT2* is closely related to the metastasis of CRC.

Metabolic reprogramming is a common feature of cancer cells, among which, lipid metabolic reprogramming has received increasing attention because of its critical role in the development and progression of cancer⁴⁰. The ability of cancer cells to rewire their lipid metabolism provides them with fatty acids for the building blocks of membranes, energy sources and signal transduction⁷. Like many other tumors, CRC shows a lipogenic phenotype with profound changes in synthesis of fatty acids⁴¹. In the present study, we found that there was a clear correlation between enhanced lipid metabolism and poorer outcomes, and this correlation was associated with the expression of *FUT2*. *FUT2* knockdown markedly reduced the intracellular levels of TG, T-CHO, and FFA and the content of neutral lipids. Studies have shown that the dysregulation of lipid metabolism in many

cancers is linked to elevated de novo fatty acid synthesis, and related enzymes, such as *FASN*, *ACC1* and *ACLY*, are abnormally overexpressed²⁵. *FASN*, in particular, is crucial for catalyzing the de novo synthesis of fatty acids and has emerged as a key target for understanding the molecular pathways controlling CRC metastasis^{42,43}. The upregulated expression of *ACC1* could promote cancer cell proliferation and metastasis²⁵. Consistently, our study revealed that *FUT2* knockdown significantly inhibited de novo fatty acid synthesis by decreasing the expression of *FASN*, *ACC1* and *ACLY*, thus repressing CRC cell growth and metastasis. *CPT1A*, a subtype of the *CPT1* transport system, plays a critical role in fatty acid oxidation, controlling the transport of fatty acids into the mitochondria for oxidation, which provides intermediate metabolites and energy to support cell proliferation^{44,45}. Here, we found that the knockdown of *FUT2* led to reduction in the expression of *CPT1A*, which might lead to the attenuation of fatty acid utilization and elimination of the proliferation of CRC cells. Furthermore, *FUT2* knockdown enhances lipid peroxidation and ferroptosis in CRC cells. Ferroptosis sensitivity in cells hinges on peroxidized polyunsaturated fatty acid levels and related enzymes, which are essential for lipid metabolism homeostasis⁴⁶, whereas the role of *FUT2* in regulation of CRC cell ferroptosis is unexplored.

The regulation of lipid metabolism is complex in cancer cells. Research has shown that oncogenic pathways can directly regulate lipid metabolism programming¹¹. Recent studies have revealed that *YAP/TAZ* can reform intracellular metabolic programs via transcriptional regulation and accelerate lipid accumulation in cancer⁴⁷. In the present study, we found a strong link between *FUT2* and the Hippo signaling pathway in CRC via bioinformatic analysis. The present study revealed that *FUT2*-mediated fucosylation promotes the translocation of *YAP1* to nucleus by inhibiting phosphorylation of *YAP1*. Meanwhile, the expression of *TAZ*, a homolog of *YAP* and interacted with *YAP* as a functional unit, was decreased by *FUT2* knockdown in CRC cells. The activated *YAP/TAZ* promotes the fatty acid synthesis and cytoskeleton formation in CRC cells, enhancing their migration and invasion of CRC cells. The conversion of glucose into fatty acids is crucial for both energy storage and metabolism regulation⁴⁸. Recently, studies have shown that active *YAP* increases the glucose utilization by promoting the transcription of glucose transporter 3 (*GLUT3*)⁴⁷. Our study revealed that the transcription of *GLUT1* was upregulated by *FUT2* via the *YAP* signaling pathway, which increased glucose uptake to support fatty acid synthesis and accumulation. *SREBP-1*, an important transcription factor in the novo synthesis of FAs, can promote the transcriptional expression of multiple enzymes, including *FASN*, *ACC1* and *SCD*⁴⁰. *SREBP-1* also serves as a critical glucose sensor, playing a vital role in bridging glucose metabolism and de novo fatty acid synthesis⁴⁹. Our study revealed that *SREBP-1* expression is not affected by *FUT2* knockdown in CRC cells; however, m*SREBP-1* expression was significantly reduced by *FUT2* knockdown. Further study revealed that *FUT2* stabilizes m*SREBP-1* by fucosylation, which enhances de novo fatty acid synthesis.

Over the past decade, many strategies have been evaluated for targeting glycosylation to control cancer progression and prevent metastasis⁵⁰. In our study, *FUT2* acted as an oncogene in CRC, enhancing de novo fatty acid biosynthesis which in turn promoted CRC cell proliferation and metastasis



through YAP1/TAZ signaling and SREBP-1. Furthermore, a prognostic model for CRC was constructed on the basis of *FUT2*, *SREBP-1*, *FASN*, and *YAP1*, and showed a high accuracy for predicting the OS of patients with CRC. Overall, these findings also imply that *FUT2* might be a potential therapeutic target for CRC.

Materials and methods

Data collection and analysis

We acquired genomic data for colorectal adenocarcinoma (COAD) and rectum adenocarcinoma (READ) along with corresponding clinical information from the TCGA through UCSC Xena (<http://xena.ucsc.edu/>).

Fig. 6 | FUT2 promotes fatty acid synthesis in CRC cells via fucosylation of YAP1. **A** Co-immunoprecipitation assay to determine the interaction between FUT2 and YAP1/TAZ in SW480 cells, indicating direct protein-protein interactions of FUT2 with YAP1. **B** SW480 cells were transfected with FUT2-shRNA or treated with 1 μ M 2F-PAF for 24 h. Following the treatment, western blot analysis of YAP1 expressions were assessed after UEA-1 pull-down. **C** Visualization of the glycosylation sites on YAP1 and SREBP-1, showing the potential sites of modification. **D** SW480 cells were transfected with FUT2-shRNA. After transfection, the cells were treated with 1 μ M 2F-PAF for 24 h, and then western blot analysis of CTGF and p-YAP1 expressions were determined. The relative density of protein bands was quantified, normalized to β -actin, and fold changes were shown in histograms from three independent experiments. **E** SW480 cells were transfected with FUT2-shRNA and YAP1-siRNA. After transfection, cells were analyzed for western blot analysis of indicated proteins. The relative density of protein bands was quantified, normalized to β -actin, and fold changes were shown in histograms from three independent experiments. **F** SW480 cells were transfected with YAP1-siRNA, and then the mRNA levels of YAP1, FASN,

and CPT1A were assessed by qRT-PCR. Data shown are mean \pm SD; $n = 3$ samples. **G, H** SW480 cells were transfected with FUT2/Lv105. After transfection, cells were treated with verteporfin (500 nM) for 24 h, and then then stained with Nile red (**G**) or phalloidin (**H**) to evaluate intracellular cytoskeleton organization. Green or red fluorescence signals were captured and visualized through a fluorescent microscope using constant fluorescence parameters explained in the methods section: scale bar, 50 μ m. **I** Design of the tumor-establishment studies. BALB/c nude mice were subcutaneously implanted with the indicated FUT2-knockdown (sh-FUT2 SW480) or control SW480 (shRNAcont) cells. **J** After 30 days of transplantation, western blot analysis of ACC1, FASN, YAP1, and TAZ expression in isolated tumors ($n = 6$ mice/group) from the SW480 xenograft model were determined. The relative density of protein bands was quantified, normalized to β -actin, and fold changes were shown in histograms from three independent experiments. Statistical significance was determined using one-way ANOVA using the Bonferroni post-hoc test, with * $p < 0.05$, ** $p < 0.01$, *** $p < 0.001$, **** $p < 0.0001$, ns: not significant.

The genomic data of colorectal tissue from 384 healthy people were obtained from the GTEx database. After elimination of expression, missing survival data, and different batches of data from the same patient, 975 samples were collected, including 616 tumor samples and 359 normal samples. The “tidyverse” and “dplyr” packages were employed for efficient data cleaning and ID conversion in R (version 4.3.2). To assess the tumor environment, the ESTIMATE algorithm was used to estimate tumor purity and quantify the abundance of infiltrating stromal and immune cells. We utilized the “limma” package⁵¹ to identify DEGs between the high- and low-FUT2 expression groups. The criteria for determining DEGs were a |fold change| > 1.3 and a $P < 0.05$. Survival analysis, which employs Cox regression analysis through the survival and “timeROC” packages, facilitated the construction of ROC curves to assess model accuracy. For a nuanced understanding of the biological pathways associated with the DEGs, we employed the “clusterProfiler” package for GSEA.

Acquisition and processing of single-cell data

The single-cell data utilized in this study were derived from an article published by Zhang L and other researchers titled “Single-Cell Analyses Inform Mechanisms of Myeloid-Targeted Therapies in Colon Cancer”⁵². Single-cell analysis was conducted via “Seurat v5.0.3”⁵³. In the quality control step, cells with detected gene counts greater than 300, ribosomal protein-encoding gene expression proportions greater than 3%, mitochondrial gene expression proportions less than 20%, and haemoglobin gene expression proportions less than 0.1% were retained. The “NormalizeData” function was employed for standardizing the single-cell dataset, whereas the “FindVariableFeatures” function identified 3000 variable features within the dataset. The “ScaleData” function was utilized to scale the data, mitigating the effects of varying sequencing depths across different cells. Cell clustering and cell type identification were performed via the “FindClusters” function. Cell type annotation genes were obtained from Cell Marker 2.0 (<http://117.50.127.228/CellMarker/>).

Cell culture

HEK293T, SW480 and DLD-1 cells were obtained from the Cell Bank of the Chinese Academy of Sciences. They were maintained in DMEM (or RPMI-1640) (Gibco, USA) supplemented with 10% FBS (Clark Bioscience, USA) and 1% penicillin/streptomycin (Gibco). Regular monitoring and passage ensured optimal cell growth and viability.

Transfection and plasmid construction

SW480 and DLD-1 cells were transduced with hU6-MCS-Ubiquitin-EGFP-IRES-puro-FUT2 vector (Addgene plasmid#227423) (Genechem, China). FUT2-overexpressing cells and negative control cells were obtained via the Lv105-FUT2 plasmid (Addgene plasmid#227439) or empty vector Lv105 (Genechem). Lentiviruses were produced in HEK293T cells, and the viral

supernatant was collected after 48 h. The supernatant was then used to infect SW480 and DLD-1 cells. Stable clones were established through selection with puromycin (Sigma, USA) for following experiments. YAP1- and TAZ-knockdown cells were generated via transient transfection of cells with 100 pM siRNA (Genechem) via the Lipofectamine 3000 transfection system (Thermo Fisher, USA). For details of the sequences used please see Supplementary Tab. 2.

Quantitative real-time PCR

Total RNA was isolated from CRC cell lines via TRIzol reagent (Takara, Japan). The cDNA was obtained via PrimeScript RT reagent (Vazyme, China), and qRT-PCR was performed via SYBR Green Master Mix (Vazyme). The results were normalized to GAPDH and are presented as the fold change in mRNA expression ($2^{-\Delta\Delta Ct}$). The sequences of primer used are listed in Supplementary Tab. 2.

Western blot analysis

In brief, the lysis of CRC cells was accomplished by adding 1% phenylmethanesulfonyl fluoride (PMSF) (Beyotime, China) and 2% phosphatase inhibitor (Beyotime) to RIPA buffer (Beyotime). Following separation via sodium dodecyl sulfate-polyacrylamide gel electrophoresis (SDS-PAGE), the proteins were transferred onto a polyvinylidene fluoride membrane. Rapid blocking solution (Epizyme, China) was used in TBS containing 0.1% Tween-20 to block the membranes for 1 h, which were then incubated with specific primary antibodies overnight at 4 °C and subsequently probed with a secondary antibody at room temperature for 1 h. Finally, enhanced chemiluminescence (ECL) (NCM Biotech, China) reagents were used to visualize the results on the Gel DocXR (Bio-Rad, USA), which was analyzed via Image J software. The primary antibodies used are listed in Supplementary Tab. 3.

Measurement of intracellular components

According to the manufacturer’s instruction, the levels of intracellular components, including Glu (Beyotime), FFAs (Solarbio, China), TG (Solarbio), T-CHO (Solarbio), ATP (Thermo Fisher), MDA (Solarbio), GSSG (Solarbio), and GSH (Solarbio), were meticulously quantified via specialized kits.

For the RSL3 treatment, SW480 cells were pretreated with 2 μ mol/L RSL3 (MedChemExpress, USA) for 24 h, followed by treatment with or without 1 μ mol/L ferrostatin (MedChemExpress) for another 24 h. Finally, the cells were collected for MDA assays.

ROS assay

For the assessment of ROS, the cells were treated with 100 μ mol/L DCFH-DA (Beyotime) in the absence of light for 30 min. Then, the cells were digested and collected via trypsin. Employing on-line flow cytometry

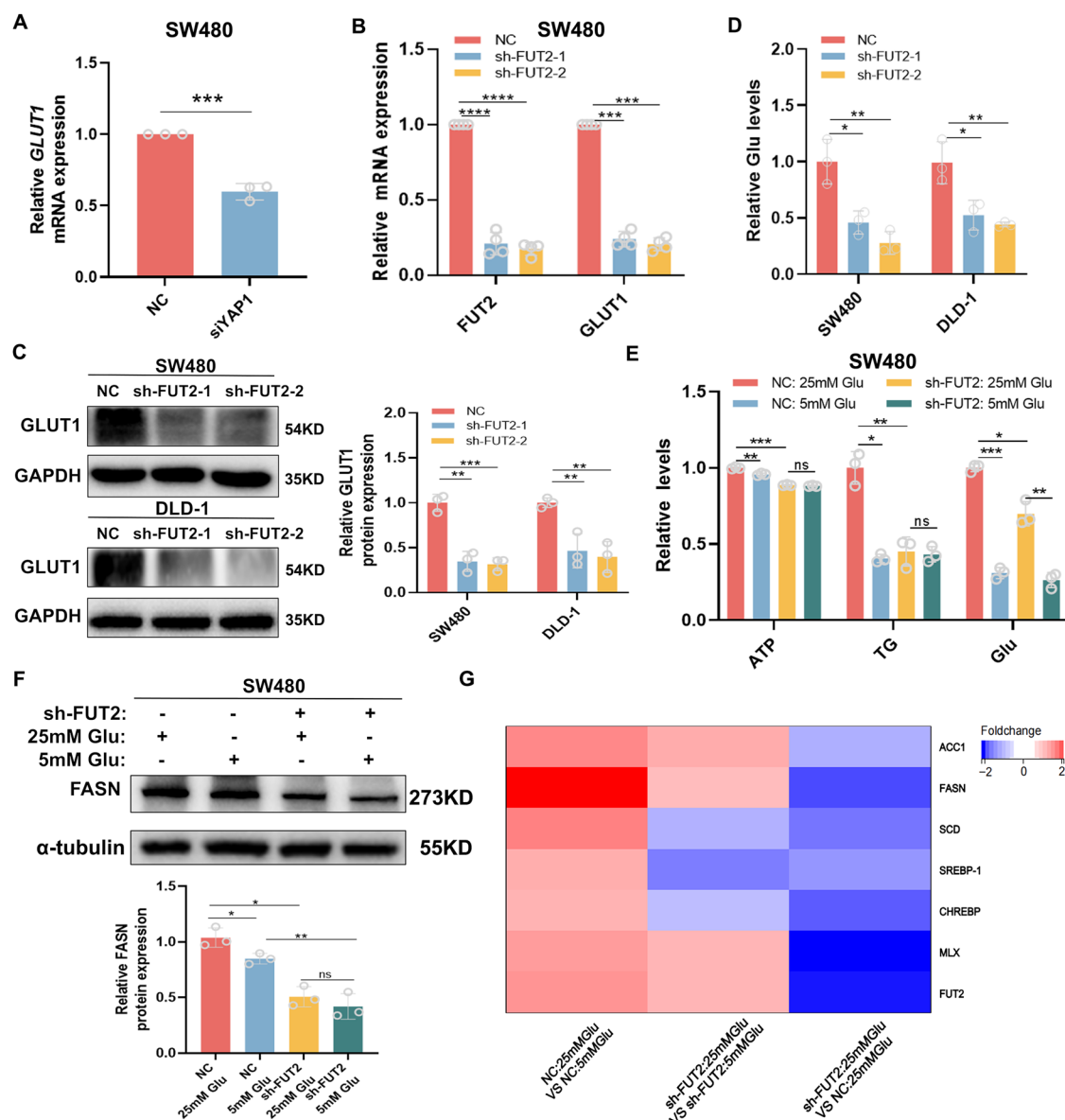


Fig. 7 | FUT2 promotes the expression of GLUT1 through YAP1 in CRC cells. SW480 cells were transfected with YAP1-siRNA (A) or FUT2-shRNA (B), and then *GLUT1* mRNA levels were assessed by qRT-PCR. Data shown are mean \pm SD; $n = 3$ samples. C SW480 and DLD-1 cells were transfected with FUT2-shRNA, and then western blot analysis of GLUT1 expressions were determined. The relative density of protein bands was quantified, normalized to GAPDH, and fold changes were shown in histograms from three independent experiments. D SW480 and DLD-1 cells were transfected with FUT2-shRNA, and then intracellular glucose (Glu) levels were assessed with detection kit. Data shown are mean \pm SD; $n = 3$ samples. E SW480 cells were transfected with FUT2-shRNA. After transfection, SW480 cells were cultured in 5 mM or 25 mM glucose media for 48 h, and then intracellular ATP, TG and Glu

levels were assessed with detection kits. Data shown are mean \pm SD; $n = 3$ samples. F SW480 cells were transfected with FUT2-shRNA. After transfection, SW480 cells were cultured in 5 mM or 25 mM glucose media for 48 h, and then western blot analysis of FASN was determined. The relative density of protein bands was quantified, normalized to α -tubulin, and fold changes were shown in histograms from three independent experiments. G SW480 cells were cultured in 5 mM or 25 mM glucose media for 48 h, and then the mRNA levels of *ACC1*, *FASN*, *SCD*, *SREBP-1*, *CHREBP*, *MLX* and *FUT2* were assessed by qRT-PCR. Data shown are mean \pm SD; $n = 3$ samples. Statistical significance was determined using one-way ANOVA using the Bonferroni post-hoc test, with * $p < 0.05$, ** $p < 0.01$, *** $p < 0.001$, **** $p < 0.0001$, ns: not significant.

(Agilent, China), the average fluorescence intensity of 2×10^4 cells was measured as a representative indicator of ROS levels. The data were processed via NovoExpress software.

Cell viability assay

SW480 cells (3×10^3) or DLD-1 cells (5×10^3) were seeded in 96-well plates in 200 μ l of medium containing 5% FBS with or without 50 μ mol/L palmitic acid (Sigma). After 24, 48 and 72 h, 10 μ l of CCK 8 (Dojindo, Japan) reagent was added to 100 μ l of the mixture, which was subsequently cultured at 37 $^\circ$ C for 2 h. The absorbance of each sample was assessed at 450 nm via an automated plate reader (Thermo Fisher).

Colony formation assay

CRC cells were cultured in 6-well plates and treated according to the experimental protocols. Two weeks later, the cells were fixed with 4% paraformaldehyde (Phygene, China), stained with crystal violet staining solution (Beyotime) for 30 min and photographed. The colony number of crystal violet stained cells was quantified using Image J software v1.6.0.

Transwell migration and invasion assays

The invasion or migration capacity of CRC cells was evaluated via Transwell membranes (Corning, USA) with or without Matrigel. In briefly, 5×10^4 cells were seeded in the upper chamber in 200 μ l of serum-free medium.

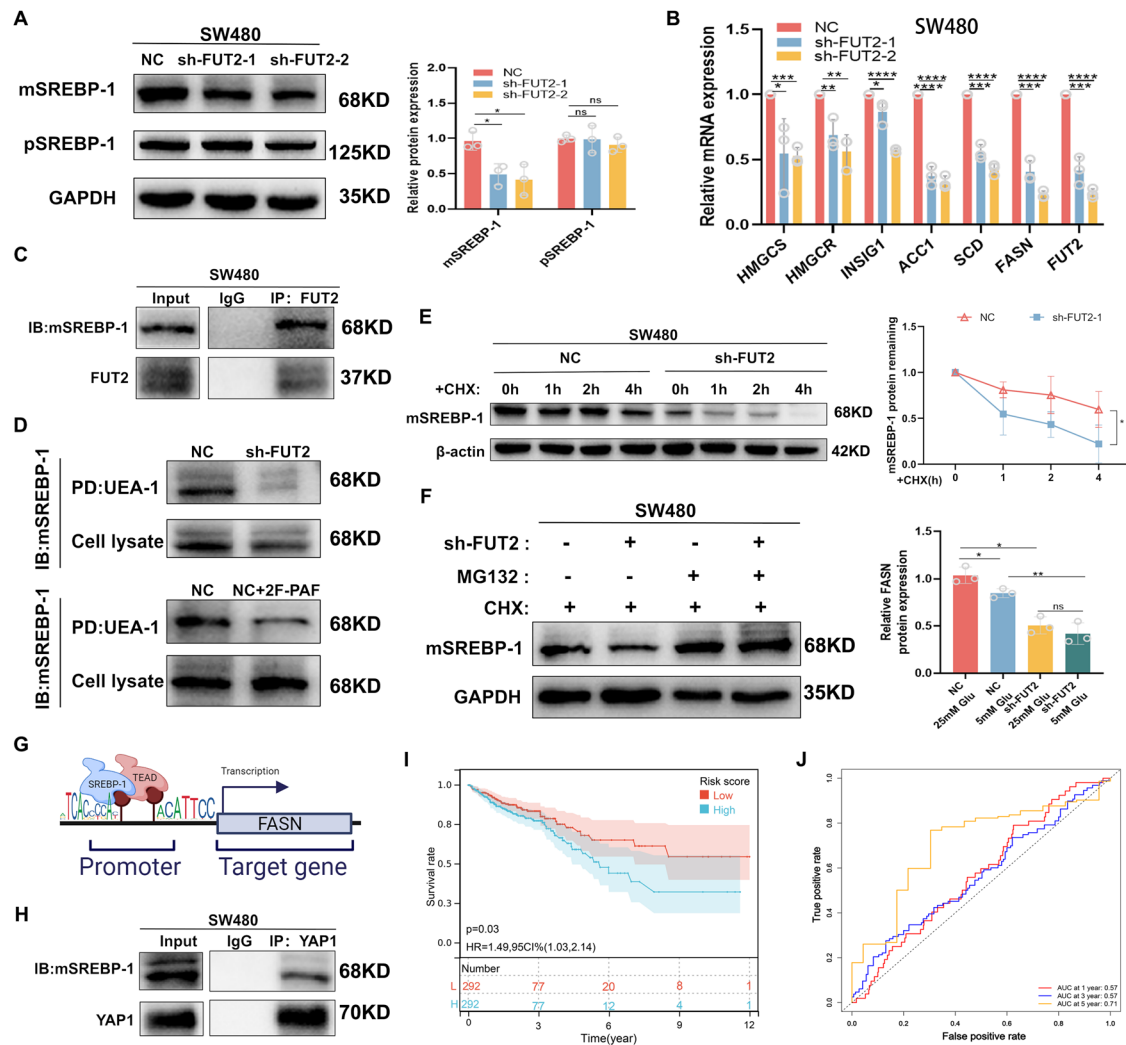


Fig. 8 | FUT2 enhances mSREBP-1 stability and promotes the de novo fatty acid synthesis. **A** SW480 and DLD-1 cells were transfected with FUT2-shRNA, and then western blot analysis of pSREBP-1 and mSREBP-1 was determined. The relative density of protein bands was quantified, normalized to GAPDH, and fold changes were shown in histograms from three independent experiments. **B** SW480 cells were transfected with FUT2-shRNA, and then the mRNA levels of *HMGCS*, *HMGCR*, *INSIG1*, *SCD*, *ACC1*, *FASN* and *FUT2* were assessed by qRT-PCR. Data shown are mean ± SD; *n* = 3 samples. **C** Co-immunoprecipitation assay was applied to determine the interaction of FUT2 and mSREBP-1 in SW480 cells. **D** SW480 cells were transfected with FUT2-shRNA or treated with 1 μM 2F-PAF for 24 h. Following the treatment, western blot analysis of mSREBP-1 was assessed after UEA-1 pull-down. **E** SW480 cells were transfected with FUT2-shRNA. After transfection, the cells were treated with 50 μM CHX for the indicated time, and then western blot analysis of mSREBP-1 expression were determined. The relative density of protein bands was quantified, normalized to β-actin, and fold changes were shown in

histograms from three independent experiments. **F** SW480 cells were transfected with FUT2-shRNA. After transfection, the cells pre-treated with CHX (50 μM) were treated with MG132 (20 μM) for 4 h. Following the treatment, cells were analyzed for Western blot. The relative density of protein bands was quantified, normalized to GAPDH, and fold changes were shown in histograms from three independent experiments. **G** Schematic representation of the predicted TEADs family and SREBP-1 in the *FASN* gene promoter. **H** Co-immunoprecipitation assay was applied to determine the interaction of mSREBP-1 and YAP1 in SW480 cells. **I** Kaplan-Meier survival curves stratified TCGA-CRC patients into high and low risk groups based on the mRNA level of *FASN*, *SREBP-1*, *YAP1*, and *FUT2*, displaying differential survival rates. **J** Time-dependent ROC curves assessed prognostic model's prognostic accuracy for CRC over 1, 3, and 5 years, presenting the AUC for each interval. Statistical significance was determined using one-way ANOVA using the Bonferroni post-hoc test, with **p* < 0.05, ***p* < 0.01, ****p* < 0.001, *****p* < 0.0001, ns: not significant.

Concurrently, 500 μl of medium supplemented with 10% FBS was placed in the lower chamber. Following a 24 h incubation at 37 °C, the cells were immobilized and photographed after they were stained with crystal violet in the chamber.

For the orlistat treatment assay, SW480 and DLD-1 cells were treated with orlistat (MedChemExpress) for 48 hours (50 μmol/L or 25 μmol/L), then the cells were subjected to migration and invasion assays. Similarly, the cells were treated with the verteporfin (MedChemExpress) for 24 h (500 nmol/L).

Immunofluorescence

For Nile red staining, the cells were treated according to the experimental instructions and stained with 0.05 μg/mL Nile red (Beyotime) at 37 °C for

10 min to visualize the lipid droplets. The cells were restrained with 1 μg/mL DAPI (Beyotime) mixed with fluorescence quencher for 1 min and then imaged under a confocal laser scanning microscope (Nikon Corporation, Japan) using a 20x objective with DAPI or Texas Red channel.

For phalloidin staining, the cells were treated according to the experimental instructions and fixed with 0.5% Triton X-100. The cells were incubated in 5 μmol/L phalloidin (Yeasen, China) for 30 min in the dark and then imaged under a confocal laser scanning microscope using a 20x objective with DAPI or FITC channel.

Co-immunoprecipitation

Proteins obtained after cell lysis were subjected to protein A + G agarose beads (Beyotime). The mixture was then incubated with the target-specific

primary antibody or with rabbit or mouse IgG as a negative control, at 4 °C for 16 h. Subsequently, protein-antibody complexes were captured using Protein A + G agarose beads pre-blocked with BSA. Following three washes with PBS, the bound proteins were collected and subsequently analyzed by Western blot.

Lectin pull-down assay

The cell lysates were incubated with UEA-1-conjugated beads (Vector Laboratories, USA) and rotated at 4 °C for 16 h. After washing several times with PBS to remove any unbound proteins, the UEA-1 enriched proteins were collected and analyzed via western blotting.

For the 2F-PAF treatment assay, SW480 cells were treated with 1 μmol/L 2F-PAF (MedChemExpress) for 24 h, then the cells were extracted for WB analysis.

Animal experiments

Animal experiments were approved by the Laboratory Animal Ethics Committee of Wenzhou Medical University and the Laboratory Animal Centre of Wenzhou Medical University (NO. WYDW2019-0245), and were performed in accordance with all relevant ethical regulations for animal use. BALB/c nude mice (female, eight weeks old) were purchased from Beijing Vital River Laboratory Animal Technology Co., Ltd. SW480-NC and SW480-sh-FUT2 cells (5×10^7) were subcutaneously injected into the right flank of BALB/c nude mice. Tumor lengths were measured with calipers every 3 days. When the maximum tumor volume reached humane endpoints (750 mm^3), euthanasia was performed on the mice (with an overdose of pentobarbital), and the tumors were then excised for imaging and weighing. A portion of the excised transplants was used for TG and T-CHO measurements, and the remaining xenografts were stored in liquid nitrogen for further experiments.

Statistical analysis

All the data were analyzed and reproduced at least three times for robustness and reproducibility. Statistical analyses were performed via R-4.3.2 and GraphPad Prism v8.0. The Wilcoxon rank test was used to analyze the distribution and expression of risk scores, stromal scores, immune scores, and gene expression across different groups. Student's *t*-test was used to compare two independent groups, whereas one-way ANOVA followed by Tukey's post hoc test was used for multiple comparisons. Bar graphs represent the mean values ± standard deviation (SD) from three independent experiments. Statistical significance was set at *P* values < 0.05.

Reporting summary

Further information on research design is available in the Nature Portfolio Reporting Summary linked to this article.

Data availability

The data generated in this study are available upon request from the corresponding author. Uncropped and unedited blot images are available in Supplementary Fig. 4. All source data underlying the graphs and charts shown in the figures are presented in Supplementary Data File 1.

Received: 6 June 2024; Accepted: 30 September 2024;

Published online: 10 October 2024

References

- Bray, F. et al. Global cancer statistics 2018: GLOBOCAN estimates of incidence and mortality worldwide for 36 cancers in 185 countries. *CA Cancer J. Clin.* **68**, 394–424 (2018).
- O'Sullivan, D. E. et al. Risk Factors for Early-Onset Colorectal Cancer: A Systematic Review and Meta-analysis. *Clin. Gastroenterol. Hepatol.* **20**, 1229–1240.e1225 (2022).
- Rawla, P., Sunkara, T. & Barsouk, A. Epidemiology of colorectal cancer: incidence, mortality, survival, and risk factors. *Gastroenterol. Rev./Przegląd Gastroenterologiczny.* **14**, 89–103 (2019).
- Ciardiello, F. et al. Clinical management of metastatic colorectal cancer in the era of precision medicine. *CA: A Cancer J. Clinicians.* **72**, 372–401 (2022).
- Zhang, C. et al. Cancer-derived exosomal HSPC111 promotes colorectal cancer liver metastasis by reprogramming lipid metabolism in cancer-associated fibroblasts. *Cell Death Dis.* **13**, 57 (2022).
- Siegel, R. L., Wagle, N. S., Cercek, A., Smith, R. A. & Jemal, A. Colorectal cancer statistics, 2023. *CA Cancer J. Clin.* **73**, 233–254 (2023).
- Yang, Y. et al. SLC25A1 promotes tumor growth and survival by reprogramming energy metabolism in colorectal cancer. *Cell Death Dis.* **12**, 1108 (2021).
- Luo, X. et al. Emerging roles of lipid metabolism in cancer metastasis. *Mol. cancer* **16**, 76 (2017).
- Yoshida, G. J. Metabolic reprogramming: the emerging concept and associated therapeutic strategies. *J. Exp. Clin. Cancer Res.* **34**, 111 (2015).
- Sedlak, J. C., Yilmaz, Ö. H. & Roper, J. Metabolism and Colorectal Cancer. *Annu Rev. Pathol.* **18**, 467–492 (2023).
- Koundouros, N. & Poulogiannis, G. Reprogramming of fatty acid metabolism in cancer. *Br. J. Cancer* **122**, 4–22 (2020).
- La Vecchia, S. & Sebastián, C. Metabolic pathways regulating colorectal cancer initiation and progression. *Semin Cell Dev. Biol.* **98**, 63–70 (2020).
- Reilly, C., Stewart, T. J., Renfrow, M. B. & Novak, J. Glycosylation in health and disease. *Nat. Rev. Nephrol.* **15**, 346–366 (2019).
- Madunić, K. et al. Colorectal cancer cell lines show striking diversity of their O-glycome reflecting the cellular differentiation phenotype. *Cell Mol. Life Sci.* **78**, 337–350 (2021).
- Singh, J. P., Zhang, K., Wu, J. & Yang, X. O-GlcNAc signaling in cancer metabolism and epigenetics. *Cancer Lett.* **356**, 244–250 (2015).
- Sun, R., Kim, A. M. J. & Lim, S.-O. Glycosylation of immune receptors in cancer. *Cells* **10**, 1100 (2021).
- Lv, Y., Zhang, Z., Tian, S., Wang, W. & Li, H. Therapeutic potential of fucosyltransferases in cancer and recent development of targeted inhibitors. *Drug Discov. Today* **28**, 103394 (2023).
- Liu, P. et al. FUT2 promotes the tumorigenicity and metastasis of colorectal cancer cells via the Wnt/β-catenin pathway. *Int. J. Oncol.* **62**, 35 (2023).
- Koo, J. H. & Guan, K. L. Interplay between YAP/TAZ and Metabolism. *Cell Metab.* **28**, 196–206 (2018).
- Dey, A., Varelas, X. & Guan, K.-L. Targeting the Hippo pathway in cancer, fibrosis, wound healing and regenerative medicine. *Nat. Rev. Drug Discov.* **19**, 480–494 (2020).
- Meng, Z., Moroishi, T. & Guan, K.-L. Mechanisms of Hippo pathway regulation. *Genes Dev.* **30**, 1–17 (2016).
- Zou, R. et al. YAP nuclear-cytoplasmic translocation is regulated by mechanical signaling, protein modification, and metabolism. *Cell Biol. Int.* **44**, 1416–1425 (2020).
- Li, X. et al. OGT regulated O-GlcNAcylation promotes papillary thyroid cancer malignancy via activating YAP. *Oncogene* **40**, 4859–4871 (2021).
- Yu, S. et al. GALNT12 promotes fibrosarcoma growth by accelerating YAP1 nuclear localization. *Oncol. Lett.* **26**, 1–11 (2023).
- Dai, W. et al. PTPRO represses colorectal cancer tumorigenesis and progression by reprogramming fatty acid metabolism. *Cancer Commun.* **42**, 848–867 (2022).
- Seetharaman, S. & Etienne-Manneville, S. Cytoskeletal Crosstalk in Cell Migration. *Trends Cell Biol.* **30**, 720–735 (2020).
- Mollinedo, F. & Gajate, C. Lipid rafts as signaling hubs in cancer cell survival/death and invasion: implications in tumor progression and therapy: thematic review series: biology of lipid rafts. *J. Lipid Res.* **61**, 611–635 (2020).
- Zheng, J. & Conrad, M. The Metabolic Underpinnings of Ferroptosis. *Cell Metab.* **32**, 920–937 (2020).

29. Jin, X. et al. Ferroptosis: Emerging mechanisms, biological function, and therapeutic potential in cancer and inflammation. *Cell Death Discov.* **10**, 45 (2024).
30. Guo, J. et al. Ferroptosis: a novel anti-tumor action for cisplatin. *Cancer research and treatment. Off. J. Korean Cancer Assoc.* **50**, 445 (2018).
31. Kashiwara, T. et al. YAP mediates compensatory cardiac hypertrophy through aerobic glycolysis in response to pressure overload. *J. Clinical Investig.* **132**, e150595 (2022).
32. Yu, A. et al. Glucose-induced and ChREBP: MLX-mediated lipogenic program promotes hepatocellular carcinoma development. *Oncogene* **42**, 3182–3193 (2023).
33. Iizuka, K., Takao, K. & Yabe, D. ChREBP-Mediated Regulation of Lipid Metabolism: Involvement of the Gut Microbiota, Liver, and Adipose Tissue. *Front Endocrinol. (Lausanne)*. **11**, 587189 (2020).
34. Shimano, H. & Sato, R. SREBP-regulated lipid metabolism: convergent physiology - divergent pathophysiology. *Nat. Rev. Endocrinol.* **13**, 710–730 (2017).
35. Jeon, T. I. & Osborne, T. F. SREBPs: metabolic integrators in physiology and metabolism. *Trends Endocrinol. Metab.* **23**, 65–72 (2012).
36. Lu, W. et al. Reprogramming immunosuppressive myeloid cells facilitates immunotherapy for colorectal cancer. *EMBO Mol. Med.* **13**, e12798 (2021).
37. Bindeman, W. E. & Fingleton, B. Glycosylation as a regulator of site-specific metastasis. *Cancer Metastasis Rev.* **41**, 107–129 (2022).
38. Fernández-Ponce, C. et al. The role of glycosyltransferases in colorectal cancer. *Int. J. Mol. Sci.* **22**, 5822 (2021).
39. Wang, W. et al. Intestinal epithelium-specific Fut2 deficiency promotes colorectal cancer through down-regulating fucosylation of MCAM. *J. Transl. Med.* **21**, 82 (2023).
40. Pham, D. V., Tilija Pun, N. & Park, P. H. Autophagy activation and SREBP-1 induction contribute to fatty acid metabolic reprogramming by leptin in breast cancer cells. *Mol. Oncol.* **15**, 657–678 (2021).
41. Currie, E., Schulze, A., Zechner, R., Walther, T. C. & Farese, R. V. Cellular fatty acid metabolism and cancer. *Cell Metab.* **18**, 153–161 (2013).
42. Menendez, J. A. & Lupu, R. Fatty acid synthase and the lipogenic phenotype in cancer pathogenesis. *Nat. Rev. Cancer* **7**, 763–777 (2007).
43. Jiang, T. et al. The m6A modification mediated-lncRNA POU6F2-AS1 reprograms fatty acid metabolism and facilitates the growth of colorectal cancer via upregulation of FASN. *Mol. Cancer* **23**, 55 (2024).
44. Ma, Y. et al. Fatty acid oxidation: An emerging facet of metabolic transformation in cancer. *Cancer Lett.* **435**, 92–100 (2018).
45. Tang, M. et al. CPT1A-mediated fatty acid oxidation promotes cell proliferation via nucleoside metabolism in nasopharyngeal carcinoma. *Cell Death Dis.* **13**, 331 (2022).
46. Yang, W. S. & Stockwell, B. R. Ferroptosis: death by lipid peroxidation. *Trends Cell Biol.* **26**, 165–176 (2016).
47. Koo, J. H. & Guan, K.-L. Interplay between YAP/TAZ and Metabolism. *Cell Metab.* **28**, 196–206 (2018).
48. Koppenol, W. H., Bounds, P. L. & Dang, C. V. Otto Warburg's contributions to current concepts of cancer metabolism. *Nat. Rev. Cancer* **11**, 325–337 (2011).
49. Cheng, C., Geng, F., Cheng, X. & Guo, D. Lipid metabolism reprogramming and its potential targets in cancer. *Cancer Commun.* **38**, 1–14 (2018).
50. Briggs, M. T. et al. Translating N-glycan analytical applications into clinical strategies for ovarian cancer. *PROTEOMICS-Clin. Appl.* **13**, 1800099 (2019).
51. Ritchie, M. E. et al. limma powers differential expression analyses for RNA-sequencing and microarray studies. *Nucleic Acids Res.* **43**, e47–e47 (2015).
52. Zhang, L. et al. Single-cell analyses inform mechanisms of myeloid-targeted therapies in colon cancer. *Cell* **181**, 442–459. e429 (2020).
53. Butler, A., Hoffman, P., Smibert, P., Papalexi, E. & Satija, R. Integrating single-cell transcriptomic data across different conditions, technologies, and species. *Nat. Biotechnol.* **36**, 411–420 (2018).

Acknowledgements

The work was supported by the Key Discipline of Zhejiang Province in Medical Technology (First Class, Category A).

Author contributions

C.D., Y.Z., J.Z., S.C., Y.L., and Z.B. performed the experiments and analyzed the data. C.D. and Y.Z. performed most of the experiments. C.D., S.F., and X.C. conceived the ideas and supervised the study. C.D. wrote the manuscript. S.F. and X.C. revised the manuscript. All the authors have read and approved the paper.

Competing interests

The authors declare no competing interests.

Additional information

Supplementary information The online version contains supplementary material available at <https://doi.org/10.1038/s42003-024-06993-x>.

Correspondence and requests for materials should be addressed to Sairong Fan or Xiaoming Chen.

Peer review information *Communications Biology* thanks Matthias Lochner, Gurdeep Singh and the other, anonymous, reviewer for their contribution to the peer review of this work. Primary Handling Editor: Christina Karlsson Rosenthal. A peer review file is available.

Reprints and permissions information is available at <http://www.nature.com/reprints>

Publisher's note Springer Nature remains neutral with regard to jurisdictional claims in published maps and institutional affiliations.

Open Access This article is licensed under a Creative Commons Attribution-NonCommercial-NoDerivatives 4.0 International License, which permits any non-commercial use, sharing, distribution and reproduction in any medium or format, as long as you give appropriate credit to the original author(s) and the source, provide a link to the Creative Commons licence, and indicate if you modified the licensed material. You do not have permission under this licence to share adapted material derived from this article or parts of it. The images or other third party material in this article are included in the article's Creative Commons licence, unless indicated otherwise in a credit line to the material. If material is not included in the article's Creative Commons licence and your intended use is not permitted by statutory regulation or exceeds the permitted use, you will need to obtain permission directly from the copyright holder. To view a copy of this licence, visit <http://creativecommons.org/licenses/by-nc-nd/4.0/>.

© The Author(s) 2024